Progresses in the structural assessment of the central region of a HELIAS 5-B breeding blanket half sector

G. Bongioví[a]*, A. Häußler[a] and the W7-X team

[a]*Karlsruhe Institute of Technology (KIT), Institute for Neutron Physics and Reactor Technology (INR), Hermann-von-Helmholtz-Platz 1, 76344 Eggenstein-Leopoldshafen, GERMANY*

Within the framework of EUROfusion action, the HELIcal-axis Advanced Stellarator (HELIAS) is considered as a possible long-term alternative to a tokamak DEMOnstration power plant (DEMO). From the plasma physics point of view, the HELIAS 5-B is a very promising reactor concept. It consists in a large 5 field period stellarator reactor directly extrapolated from Wendelstein 7-X. Intense studies are currently ongoing at KIT in order to achieve a preliminary design of a breeding blanket (BB) for the HELIAS 5-B reactor which takes the outcomes from the pre-conceptual design of the tokamak DEMO BB into account. To this end, the Helium-Cooled Pebble Bed (HCPB) and the Water-Cooled Lithium Lead (WCLL) BB concepts have been considering, focusing on the investigation of the suitability of their main structural features to the stellarator geometry. In this regard, possible design constraints coming from the Remote Maintenance (RM) have to be fulfilled in order to better align the blanket segmentation. In the present work a more sophisticated structural assessment of the central region of a HELIAS 5-B BB half sector has been performed, paying attention to the predicted displacement field. The study has been aimed at the refinement of the numerical model so far adopted, investigating the impact of the major assumptions, such as Vacuum Vessel (VV) temperature and equivalent Young's Modulus, on the obtained results. The results are herewith presented and critically discussed, giving some hints for the follow-up of this activity.

Keywords: HELIAS, stellarator, breeding blanket, thermomechanics, FEM analysis.

1. Introduction

The European roadmap for the realization of fusion energy [1] foresees the design, construction and exploitation of the DEMO reactor in order to produce electricity by nuclear fusion in the next decades. To this purpose the DEMO reactor, conceived according to the tokamak concept, is currently being designed under the supervision of EUROfusion consortium.

In parallel, EUROfusion is also promoting studies on the stellarator concept, considered as the long term backup solution. In particular feasibility studies of the HELIAS fusion reactor [2],[3], equipped with a tritium BB, are currently ongoing even though they are in a very early stage. Nevertheless, preliminary researches are ongoing at KIT [4]-[9] in order to acquire basic results aimed at developing, in a near future, the design of a BB for the HELIAS 5-B machine. It has to be noted that these are the first-ever studies of a BB for a stellarator-type fusion reactor and, therefore, lot of assumptions have to be made due to the early stage of the activity. However, they can represent a starting point for the development of this research line.

In this framework, the present work reports the advancements in the assessment of the central region of a HELIAS 5-B half-field period aimed at defining the boundaries for future structural analysis. Indeed the design of the HELIAS 5-B BB is not mature enough to allow a full structural assessment, due to the lack of design information about cooling system, fixation/support systems, BB internal components and so on. Likewise, the extremely complicated shape of the BB segments requires, as first approach, the investigation of their global behavior in order to refine, successively, the design. Then, complete and detailed structural assessment will be performed in a further phase. Hence, at the present stage, attention is paid to the deformations arising within the BB structure in order to have an overview of the BB overall mechanical behavior under pertinent steady state loading conditions.

In particular, the work here presented is mainly due to show the displacement field arising within the BB structure because of thermal and gravity loads. The obtained results are important to preliminary assess the global behavior of the BB segments, to test the proposed BB segmentation strategy and to give hints for the definition of a proper BB remote maintenance strategy. Indeed, due to the BB segments fully 3D spline-based shape, any analytical predictions is hard to be carried out with a high confidence level.

The work here reported is on completion of the assessment already presented in [9]. Indeed, in this latter work a study concerning the far end regions of the HELIAS 5-B BB was reported. This paper is now focused on the central BB rings.

Firstly, an estimation of the BB segments [10] weight is provided. Then, a parametric analysis, aimed at verifying the impact of the assumed equivalent Young's Modulus on the BB displacement field, has been carried out. Lastly, starting from [4], a more sophisticated assessment of the BB deformation field has been performed, adopting a discrete 3D thermal field for the BB and different Vacuum Vessel temperatures.

author's email: gaetano.bongiovi@kit.edu

The study has been carried out adopting a numerical approach based on the Finite Element Method (FEM) and using the commercial ANSYS v.19.1 FEM code.

2. The HELIAS 5-B breeding blanket

A 3D geometric model of a half-field period HELIAS-5B BB sector, including the VV and dummy BB segments (fully homogenized blocks without internal details), has been considered (Fig. 1). It extends toroidally for 36° encompassing 8 BB rings which have been designed to be separated by 20 mm gaps. Each ring is composed by 5 BB segments separated, in their turn, by 20 mm gaps along poloidal direction. Each ring includes the Back Supporting Structure (BSS), the Breeding Zone (BZ), the First Wall (FW) and the 2 mm-thick tungsten armor (W) [7]. The rings are then connected to the VV, divided in inner, shielding and outer layer.

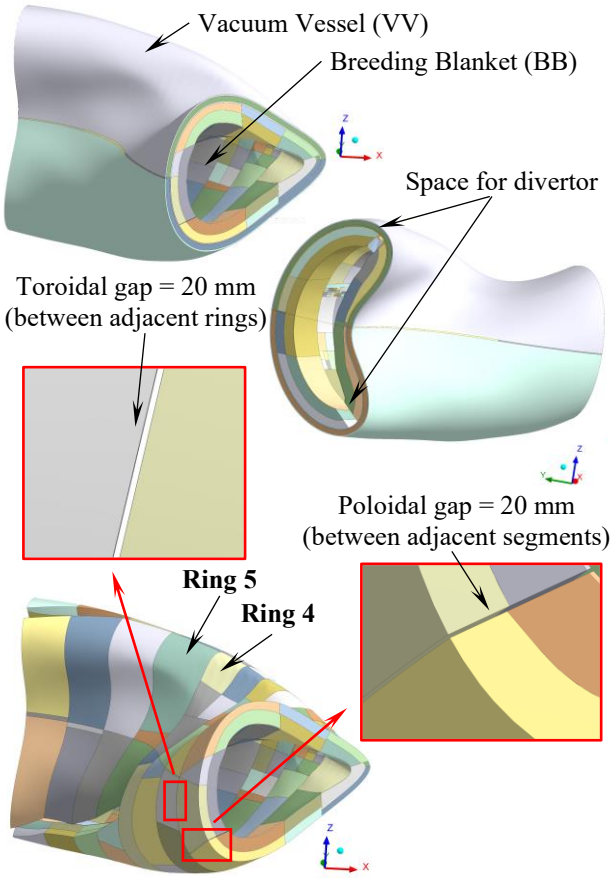

Fig. 1. The HELIAS 5-B BB half torus sector.

The central rings, namely Ring 4 and Ring 5, have been assessed in this work (Fig. 2). A geometric model comprehensive of the two rings and the proper VV portion has been purposely developed. In Fig. 2, the segments within each ring have been properly numbered to easily identify them in the following.

Eurofer steel [11] has been considered as structural material for BB segments, whereas AISI 316 steel has been assumed for the VV, including a steel-water mixture in the VV shielding layer. Moreover, the FW covering layer made of tungsten has been considered. Temperature dependent thermomechanical properties have been adopted for all the materials.

As homogenized dummy segments are considered, proper equivalent densities have been calculated and adopted in order to take the masses of the structural materials, breeder and coolant into account. To this purpose, the same material compositions [12] as the Helium-Cooled Pebble Bed [13]-[15] and Water-Cooled Lithium Lead [16]-[18] DEMO BB concepts have been assumed.

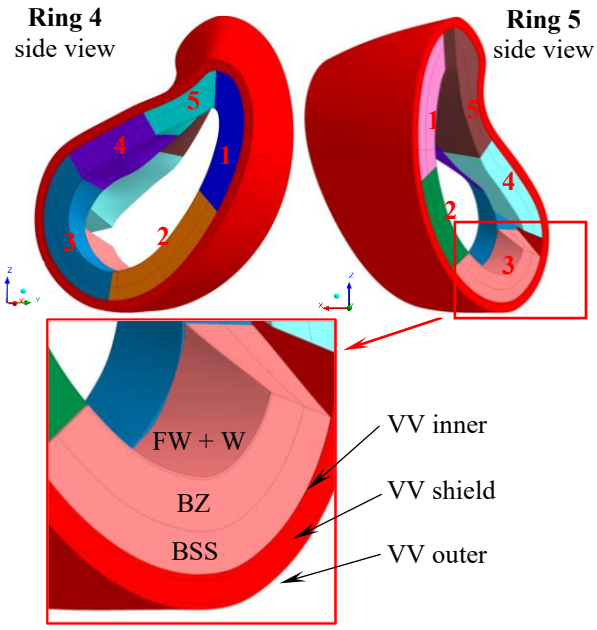

Fig. 2. Rings 4-5 geometric model.

3. Estimation of the BB segments weight

The interaction between BB and Remote Maintenance systems is crucial for their reciprocal development, both for DEMO and HELIAS. In particular, RM shall impose a limit on the BB segments weight in order to ensure that the existing tools are capable of safely handling the BB segments.

Therefore, the weight of the HELIAS 5-B BB segments belonging to Ring 4 and Ring 5 has been estimated considering HCPB and WCLL BB concepts (Table 1). The other BB concepts presently investigated in EU [19],[20] for the DEMO BB design are not considered in this study.

Table 1. Estimated BB segments weight [10^3 kg].

Segment	Ring 4		Ring 5	
	HCPB	WCLL	HCPB	WCLL
1	30.0	65.3	25.6	54.7
2	25.8	56.2	19.8	46.6
3	15.9	34.8	25.4	53.6
4	10.5	27.8	16.6	39.6
5	13.4	32.4	20.2	44.9

Results show that, for the HCPB BB, the heaviest segments are segment 1 for Ring 4 ($30.0*10^3$ kg) and segment 1 and 3 for Ring 5 ($25.6*10^3$ and $25.4*10^3$kg, respectively). As expected, higher weights are calculated for WCLL BB concept due to the presence of liquid metal.

Regarding WCLL BB concept, it has to be noted that a proper draining procedure for the working fluids (cooling water and liquid breeder) may be foreseen and, therefore, the weight to be managed by RM tools could be lower than that reported in the table. However, at the present stage, it is not clear yet if so a kind of draining could be set-up for HELIAS 5-B BB and, therefore, the segments weight reported in Table 1 is considered as an upper limit for the RM.

This preliminary evaluation represents the starting point to define the BB-RM interface following a systems engineering approach [21]-[23]. In this way a set of design constraints shared by BB and RM shall be developed in order to better orient the reciprocal design ensuring the compatibility of the two systems.

4. Parametric study of the equivalent Young's Modulus influence

In the preliminary assessments reported in [4],[5], the temperature dependent Young's Modulus E is equal to 10% of the actual one which has been used for the dummy components. This assumption, derived from the DEMO WCLL BB [24], allows to save displacement passing from the detailed structure to the dummy model.

Here, a parametric study of the assumed E value has been performed to investigate its influence on the displacement field, focusing on the variation of the residual poloidal gaps between adjacent BB segments. Temperature-dependent values of E equal to 25%, 50%, 75% and 100% of the actual ones have been considered and results have been compared. To this purpose, no W armor has been considered to be consistent with the reference case [4]. For the studies reported hereafter, only HCPB BB concept has been assessed.

4.1 The Rings 4-5 FEM model

The same FEM model already developed for the study reported in [4] has been used. Concerning the thermal state, spatially-averaged temperatures of FW, BZ, BSS and VV have been calculated from the DEMO BB thermal analysis and applied [25]-[27]. In particular, FW has been assumed at 445.8 °C, BZ at 588.0 °C, BSS at 328.5 °C and VV at 200 °C. Regarding gravity load, the global Z direction has been considered as the vertical one (Fig. 2). Lastly, a proper set of mechanical constraints has been applied to VV nodes highlighted in red in Fig. 3. All the BB components have been considered tied from the mechanical point of view.

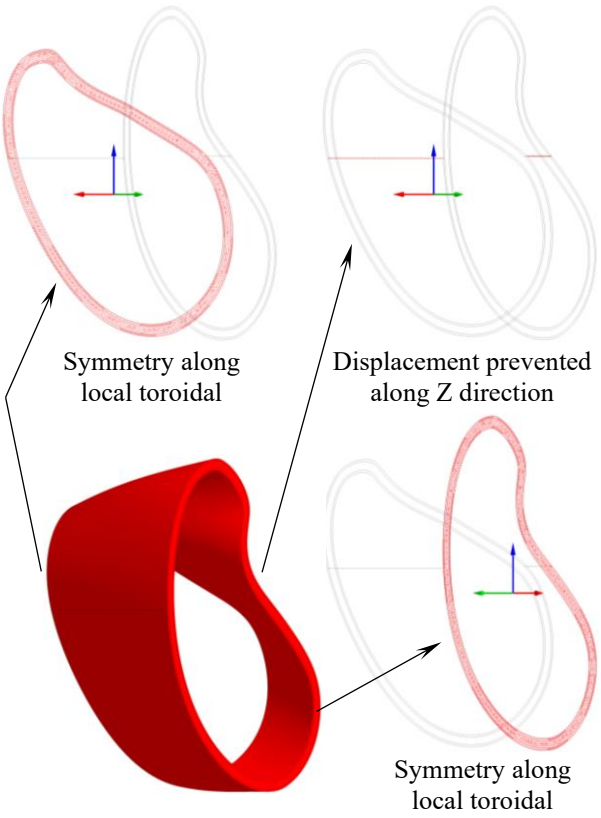

Fig. 3. Mechanical restraints.

4.2 Results of the E parametric analysis

The results in terms of minimum residual poloidal gaps in between adjacent BB segments are summarized in Table 2 and Table 3 for Ring 4 and 5, respectively.

Table 2. E parametric analysis results - Ring 4.

	Minimum residual gap [mm]				
E	Seg 1-2	Seg 2-3	Seg 3-4	Seg 4-5	Seg 5-1
10%	2.06	13.39	9.72	12.52	7.71
25%	2.18	13.39	10.71	11.95	8.25
50%	2.00	13.24	11.34	11.59	8.66
75%	1.78	13.05	11.63	11.37	8.91
100%	1.58	12.91	11.79	11.21	9.09

Table 3. E parametric analysis results - Ring 5.

	Minimum residual gap [mm]				
E	Seg 1-2	Seg 2-3	Seg 3-4	Seg 4-5	Seg 5-1
10%	3.93	8.95	-	8.57	-
25%	4.51	8.86	-	7.23	-
50%	4.60	8.75	-	6.43	-
75%	4.52	8.64	-	6.04	-
100%	4.43	8.54	-	5.80	-

The obtained results have shown that there is only a moderate influence of the assumed E values on the minimum residual gaps in poloidal direction. Hence, on the basis of these results, two limit conditions can be identified and, analogous to [9], the corresponding steady state loading scenarios have been defined and consequently called as:

- Less Conservative (LC) scenario: that one where E=10% of the actual ones are assumed.
- More Conservative (MC) scenario: that one where actual E values are assumed.

5. Assessment of Ring 4 and Ring 5 displacement field

The FEM model adopted for the *E* sensitivity study has been properly refined in order to assess more precisely the residual poloidal gaps between adjacent segments of Ring 4 and Ring 5 of the HELIAS 5-B HCPB BB. These produced modifications are widely described in the following, focusing on their impact on the results prediction.

5.1 The Rings 4-5 refined FEM model

Firstly, differently from the precious model, the refined Rings 4-5 FEM model includes the 2 mm-thick W armor. Moreover, in order to apply a discrete 3D temperature profile taken from DEMO HCPB BB thermal analysis, all the components of the geometric model shown in Fig. 2 have been purposely sliced (Fig. 4) by means of a proper campaign of geometry editing.

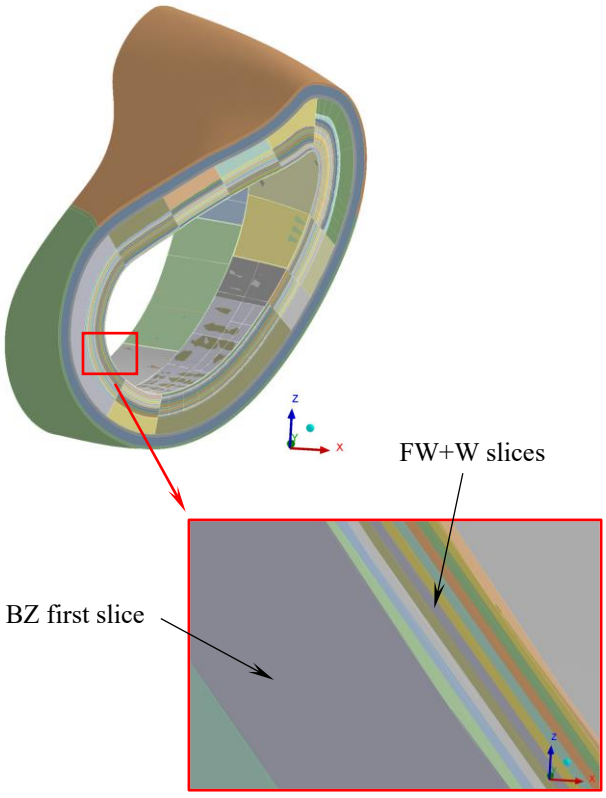

Fig. 4. Rings 4-5 with sliced components - detail of the FW.

Coherently with the less refined FEM models, linear tetrahedral elements have been chosen for the mesh. In particular, for the refined model a mesh of ~2.2 M nodes connected in ~8.4M elements has been set-up (Fig. 5). The selected grid ensures a good compromise between the calculation time and results accuracy.

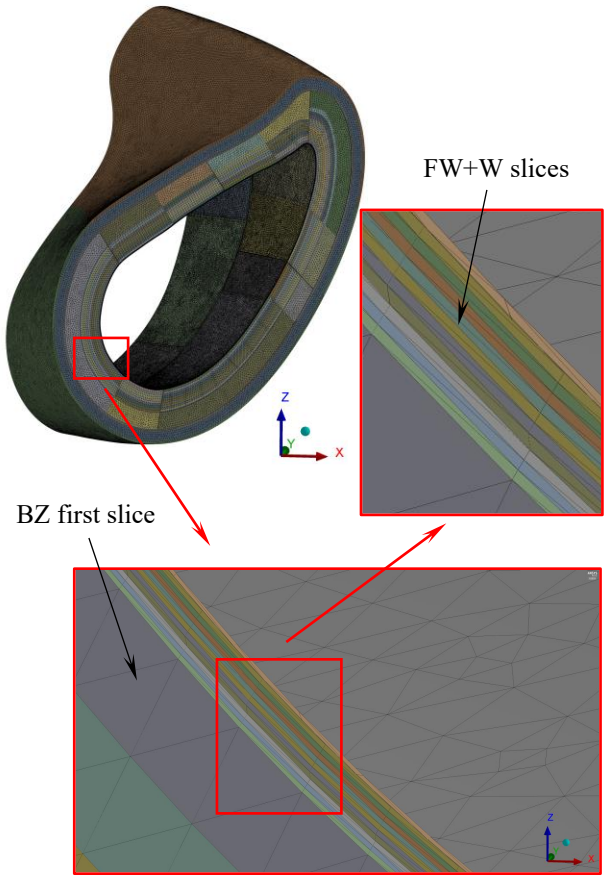

Fig. 5. Rings 4-5 with sliced components - mesh.

As to the adopted spatial temperature distribution, the W armor has been assumed at 551.4 °C. Differently from the previous investigations, properly calculated average temperatures have been imposed to each FW, BZ and BSS slice instead of to the full component. As an example, the assumed FW temperature profile is reported in Table 4. Since the FW is 25 mm thick in all the segments of Ring 4 and Ring 5, the same temperature profile has been imposed to all of them. This is not valid for BZ and BSS due to the different thicknesses between the segments. This means that varying temperature profiles have been calculated, based on the geometry segmentation, and applied.

Table 4. FW 3D discrete temperature profile.

r [mm]	T [°C]	r [mm]	T [°C]
0-2.5	544.8	12.5-15	400.2
2.5-5	510.8	15-17.5	403.7
5-7.5	470.2	17.5-20	415.5
7.5-10	431.6	20-22.5	430.6
10-12.5	408.3	22.5-25	442.4

As to VV, its three regions (inner, shield and outer VV) have been assumed at different temperatures in order to simulate the thermal gradient arising within this component. In particular, due to recent studies performed in the framework of DEMO VV design, two different

cases have been considered:

- Hot VV case [28]: characterized by VV outer at 180 °C, VV shield at 205 °C and VV inner at 230 °C.
- Cold VV case [29]: characterized by VV outer at 40 °C, VV shield at 65 °C and VV inner at 90 °C.

Lastly, gravity load has been taken into account considering the global Z direction as the vertical one.

As far as mechanical restraints are concerned, the same boundary conditions depicted in Fig. 3 have been maintained.

Hence, Ring 4 and Ring 5 structural performances have been investigated in the following four steady state loading scenarios:

- LC+Hot VV (E =10%, VV between 180 and 230 °C)
- MC+Hot VV (E =100%, VV between 180 and 230 °C)
- LC+Cold VV (E =10%, VV between 40 and 90 °C)
- MC+Cold VV (E =100%, VV between 40 and 90 °C)

Attention has been mainly paid to the resulting displacement fields, focusing on the residual gaps along both poloidal and toroidal direction. Moreover, the toroidal displacement towards the adjacent rings (namely towards Ring 3 and Ring 6, not included in the model) has been investigated. Lastly, the poloidal displacement of Ring 5 segments facing the divertor openings has been assessed as well in order to have an idea of the BB mechanical behavior also in these regions.

5.2 Results

Adopting the above-mentioned four steady state loading scenarios and the refined model set-up, proper structural analyses have been performed with paying attention to the obtained displacement field. In particular, displacement along poloidal and toroidal directions have been assessed.

5.2.1 Displacement along poloidal direction

The obtained results in terms of minimum residual poloidal gaps for Ring 4 are presented, as to LC scenarios, in Table 5 and, concerning MC scenarios, in Table 6. Negative values (in red) mean that overlapping occurs, whereas those values lower than 5 mm (assumed as the lowest desirable minimum residual gap to cope with tolerances) are reported in blue. Looking at the column "Δ%" of both tables, it presents the percentage variation of the minimum residual gaps due to the change in VV temperature.

Results clearly show that, in both LC and MC scenarios, the cold VV acts like a rigid wall towards BB and overlapping can occur. In fact, due its low temperature, the cold VV does not accommodate the BB segments thermal expansion. Thus, BB can only move towards the plasma chamber and this effect results in a significant reduction of the gaps between adjacent segments. On the contrary, hot VV cases are safe (i.e. no overlapping predicted) even though very narrow residual gaps have been calculated for segment 1-2 in both LC and MC scenarios.

Table 5. Ring 4 results - LC scenarios ($\boldsymbol{E}$ =10%).

	Minimum residual gap [mm]		
Segment	LC+Cold VV	LC+Hot VV	Δ%
1-2	-9.126	3.053	133.5
2-3	2.963	10.112	241.3
3-4	6.953	11.949	71.8
4-5	2.734	9.476	246.6
5-1	-0.639	8.237	1389.7

Table 6. Ring 4 results - MC scenarios ($\boldsymbol{E}$ =100%).

	Minimum residual gap [mm]		
Segment	MC+Cold VV	MC+Hot VV	Δ%
1-2	-9.393	0.429	104.6
2-3	6.300	10.587	68.0
3-4	8.798	12.145	38.0
4-5	3.981	9.072	127.9
5-1	0.077	6.837	8825.6

In Table 7, the influence of the E value in case of hot VV is summarized. The maximum percentage variation (~86%) between LC and MC scenario is predicted for segment 1-2. For segment 2-3, 3-4 and 4-5 interfaces no significant variation has been calculated instead. Finally, a moderate influence on segment 5-1 residual gap of the E value has been carried out.

Table 7. Ring 4 results - Hot VV cases.

	Minimum residual gap [mm]		
Segment	LC+Hot VV	MC+Hot VV	Δ%
1-2	3.053	0.429	-85.9
2-3	10.112	10.587	4.7
3-4	11.949	12.145	1.6
4-5	9.476	9.072	-4.3
5-1	8.237	6.837	-17.0

Similar behavior has been predicted for Ring 5 segments, as shown in Table 8 (for LC scenarios) and Table 9 (for MC scenarios). The effect of the VV low temperature is clear for this BB ring, too. In Table 10, the influence of E value in case of hot VV condition is highlighted. As it can be observed, the maximum percentage variation of the minimum residual gaps is of ~36 % (segment 4-5 interface). As to segment 1-2, a remarkable impact of the assumed Young's Modulus in case of hot VV has been predicted, whereas a moderate influence has been found for segment 2-3 gap.

Table 8. Ring 5 results - LC scenarios ($\boldsymbol{E}$ =10%).

	Minimum residual gap [mm]		
Segment	LC+Cold VV	LC+Hot VV	Δ%
1-2	-4.209	5.749	236.6
2-3	-0.494	7.934	1707.4
4-5	-3.198	5.944	285.9

Table 9. Ring 5 results - MC scenarios ($\boldsymbol{E}$ =100%).

	Minimum residual gap [mm]		
Segment	MC+Cold VV	MC+Hot VV	Δ%
1-2	-3.964	3.968	200.1
2-3	0.962	7.196	648.0
4-5	-4.258	3.829	189.9

Table 10. Ring 5 results - Hot VV cases.

Minimum residual gap [mm]			
Segment	LC+Hot VV	MC+Hot VV	Δ%
1-2	5.749	3.968	-31.0
2-3	7.934	7.196	-9.3
4-5	5.944	3.829	-35.6

As an example, the total displacement field obtained in MC+Hot VV scenario is presented in Fig. 6 for the Ring 4 in side view. Here, details of the segment 1-2 interface of Ring 4 are also shown, superimposing the undeformed wireframe to the deformed structure, in order to visualize the smallest minimum residual gap (equal to 0.429 mm) for this ring.

Similarly, in Fig. 7 the same total displacement field is shown for Ring 5 in side view with a detailed picture of the segment 4-5 interface, obtained by superimposing the undeformed wireframe to the deformed structure, too. In this way, the smallest minimum residual gap (equal to 3.829 mm) calculated for this ring can be shown.

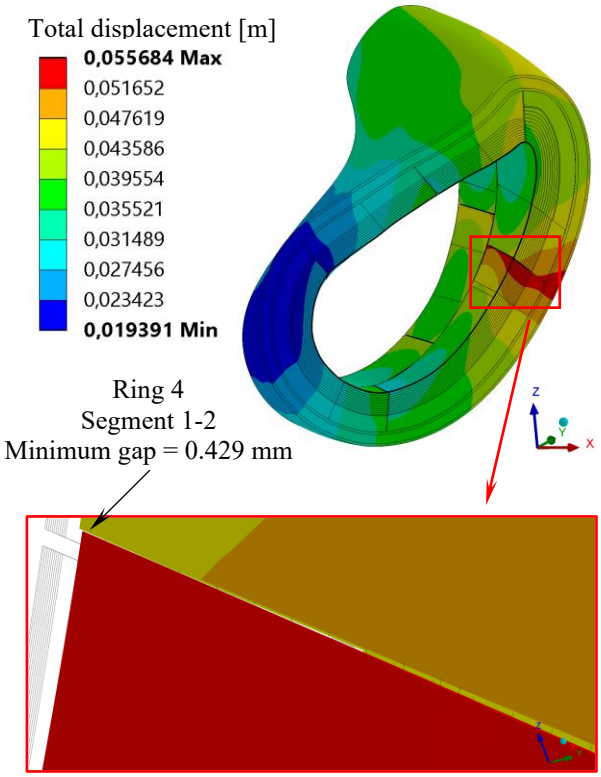

Fig. 6. Ring 4-5 - MC+Hot VV scenario - Total displacement.

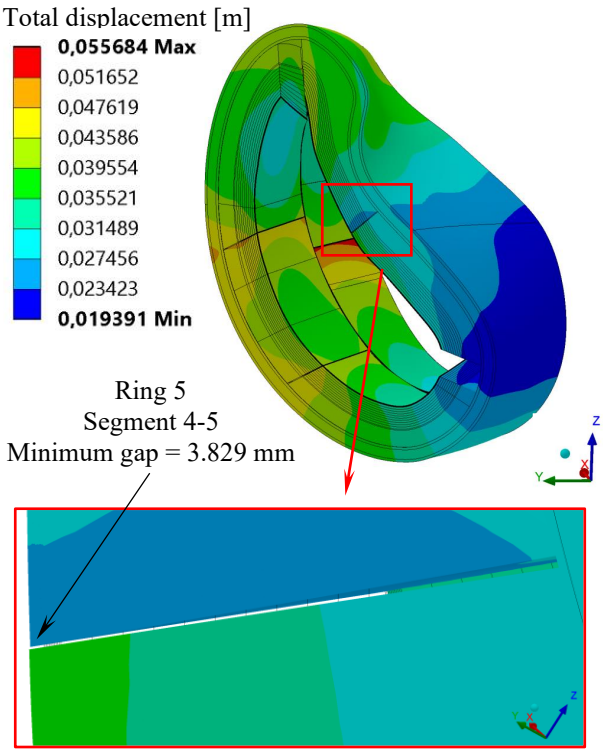

Fig. 7. Ring 4-5 - MC+Hot VV scenario - Total displacement.

As Ring 5 houses the openings for the divertor, the maximum poloidal displacement of segment 1, 3, 4 and 5 faces towards these divertor openings has been reported in Table 11 and Table 12. Negative values means that the maximum poloidal displacement is opposite to the divertor opening. As an example, the total displacement field in MC+Hot VV scenario is reported in Fig. 8 with the details of BB regions facing the divertor openings. In this detailed picture, the undeformed wireframe has been superimposed to the deformed structure.

It has to be noticed that, currently, no studies are ongoing for the divertor design. Hence, the following outcomes might be taken into account, in the future, for its development.

Table 11. Ring 5 maximum poloidal displacement towards divertor openings - LC scenarios (***E*** =10%).

Maximum poloidal displacement [mm]			
Segment	LC+Cold VV	LC+Hot VV	Δ%
1	6.422	-28.951	-550.82
3	4.268	-6.963	-263.16
4	10.854	14.070	29.63
5	18.556	40.963	120.75

Table 12. Ring 5 maximum poloidal displacement towards divertor openings - MC scenarios (***E*** =100%).

Maximum poloidal displacement [mm]			
Segment	MC+Cold VV	MC+Hot VV	Δ%
1	3.639	-25.798	-808.95
3	0.631	-7.453	-1281.10
4	11.742	14.303	21.81
5	20.775	39.820	91.67

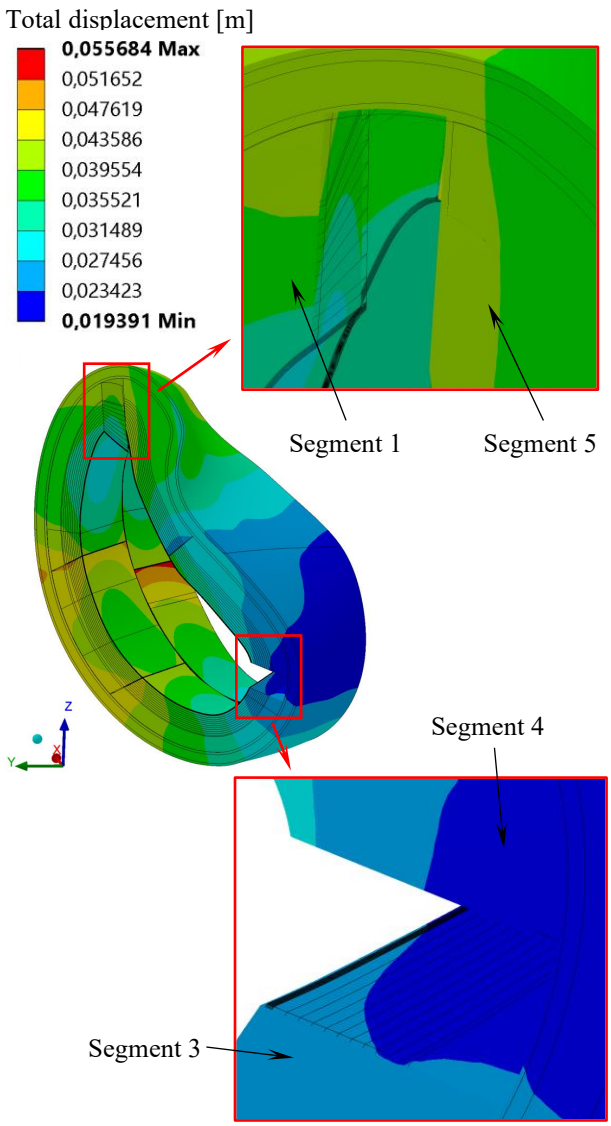

Fig. 8. Ring 4-5 - MC+Hot VV scenario - Total displacement.

5.2.2 Displacement along toroidal direction

As far as toroidal displacement is concerned, the potential overlapping occurring along toroidal direction in between Ring 4 and Ring 5 has been investigated. To this end, the minimum residual toroidal gap, calculated in the four considered loading scenarios, is reported in Table 13. Also for toroidal gap the hot VV condition ensures the highest minimum residual gap amounts, which are above the recommended limit of 5 mm.

Table 13. Ring 4-5 results - Minimum residual toroidal gap.

Scenario	Minimum residual toroidal gap [mm]
LC+Cold VV	4.591
LC+Hot VV	10.270
MC+Cold VV	4.683
MC+Hot VV	9.680

Lastly, the maximum toroidal displacement of Ring 4 and Ring 5 segments towards, respectively, Ring 3 and Ring 6 are reported from Table 14 to Table 17. Almost all the predicted values are well below 10 mm, namely lower than the half of the initial gap of 20 mm.

Table 14. Ring 4-5 results - Maximum toroidal displacement.

Maximum toroidal displacement [mm] - LC+Hot VV		
Segment	Ring 4	Ring 5
1	6.118	4.346
2	4.203	3.683
3	3.164	4.558
4	3.037	4.844
5	6.086	3.936

Table 15. Ring 4-5 results - Maximum toroidal displacement.

Maximum toroidal displacement [mm] - LC+Cold VV		
Segment	Ring 4	Ring 5
1	10.109	6.957
2	6.809	5.960
3	4.993	7.072
4	4.963	7.239
5	9.677	6.726

Table 16. Ring 4-5 results - Maximum toroidal displacement.

Maximum toroidal displacement [mm] - MC+Hot VV		
Segment	Ring 4	Ring 5
1	6.597	4.288
2	4.281	3.422
3	3.327	4.678
4	3.129	5.167
5	6.360	4.068

Table 17. Ring 4-5 results - Maximum toroidal displacement.

Maximum toroidal displacement [mm] - MC+Cold VV		
Segment	Ring 4	Ring 5
1	9.851	6.175
2	6.346	5.042
3	4.835	6.552
4	4.944	7.048
5	9.248	6.272

5.2.3 Summary

Trying to summarize the obtained results, one can state that the outcomes are promising and encourage the further continuation of this assessment on the basis of the proposed segmentation strategy. Anyway, it has to be noticed that some narrow minimum residual gaps are calculated also in the hot VV cases for both Ring 4 and Ring 5. This suggests to further developing the BB segments design to achieve better performances.

At the same time, these results allow concluding that the VV temperature could represent a major constraint for the development of the HELIAS 5-B BB design. An attachment system could be necessary to decouple the VV and BB, reducing the influence of VV deformation on the BB structural performances. Lastly, the impact of the assumed mechanical restraints have to be carefully investigated. To this end, larger numerical models reproducing wider BB regions (and possibly the whole 72° toroidal sector) should be set-up.

6. Conclusion

Within the framework of the EUROfusion consortium, a research activity is ongoing at KIT to assess the feasibility of the BB for the HELIAS 5-B stellarator fusion reactor. Structural calculations of some of the most representative BB rings have been performed adopting detailed homogenized FEM models.

The quite promising outcomes encourage the follow-up of the activity based on the current proposed BB segmentation strategy. A direct follow-up could be the assessment of the whole BB sector, extending to a 72° model in toroidal direction. Moreover, since a strong influence of the VV temperature on the BB structural performances has been found, the development of an attachment system devoted to connect BB and VV is crucial.

Another important aspect to be addressed in the next step is the design of the BB internal components (i.e. stiffening plates [30], FW channels [31] and caps [32]), in order to attain a fully HELIAS relevant thermal and mechanical BB characterization. Lastly, preliminary estimation of the BB segments dead weight has been provided in order to define the RM-BB interface.

Acknowledgment

This work has been carried out within the framework of the EUROfusion Consortium and has received funding from the Euratom research and training programme 2014-2018 and 2019-2020 under grant agreement No 633053. The views and opinions expressed herein do not necessarily reflect those of the European Commission.

References

[1] T. Donné et al., European Research Roadmap to the Realisation of Fusion Energy, EUROfusion, 2018 (ISBN 978-3-00-061152-0).

[2] F. Schauer et al., HELIAS 5-B magnet system structure and maintenance concept, Fus. Eng. Des. 88 (2013) 1619-1622.

[3] F. Warmer et al., From W7-X to a HELIAS fusion power plant: On engineering considerations for next-step stellarator devices, Fus. Eng. Des. 123 (2017) 47-53.

[4] G. Bongiovì et al., Preliminary structural assessment of the HELIAS 5-B breeding blanket, Fus. Eng. Des., https://doi.org/10.1016/j.fusengdes.2018.11.027, 2018.

[5] U. Fischer et al., Nuclear design issues of a stellarator fusion power plant with breeder blanket in comparison to tokamaks, paper presented at 27th IAEA Fusion Energy Conference (FEC 2018).

[6] A. Häußler et al., Use of mesh based variance reduction technique for shielding calculations of the stellarator power reactor HELIAS, Fus. Eng. Des., https://10.1016/j.fusengdes.2019.01.052, 2019.

[7] A. Häußler et al., Neutronics analyses for a stellarator power reactor based on the HELIAS concept, Fus. Eng. Des., 136, pp. 345-349, 2018.

[8] A. Häußler et al., Verification of different Monte Carlo approaches for the neutronic analysis of a stellarator, Fus. Eng. Des., 124, pp. 1207-1210, 2017.

[9] G. Bongioví et al., Advancements in the HELIAS 5-B breeding blanket structural analysis, contribution at the 14th International Symposium on Nuclear Fusion Technology, Budapest, 22-27 Septermber 2019.

[10] G. Bongiovì et al., Multi-Module vs. Single-Module concept: Comparison of thermomechanical performances for the DEMO Water-Cooled Lithium Lead breeding blanket, Fus. Eng. Des., 2018, 136 Part B, pp. 1472-1478.

[11] Final Report on the EFDA Article 7 contract EFDA/06-1903 on "Procurement of reduced activation ferritic-martensitic steel type 9CrWTaV (EUROFER) for the TBM fabrication technology trials and mock-ups", Saarschmiede GmbH, July 2009.

[12] G. A. Spagnuolo, EFDA_D_2N5LUV v1.0 - Blanket Material Composition For Neutronics - January2017, IDM document ref. 2N5LUV.

[13] F. Hernández et al., A new HCPB breeding blanket for the EU DEMO: Evolution, rationale and preliminary performances, Fus. Eng. Des. 124 (2017) 882-886.

[14] F. Hernández et al., Overview of the HCPB Research Activities in EUROfusion, IEEE Trans. on Pl. Sc. 46 (2018) 2247-2261.

[15] F. Hernández et al., Advancements in the Helium-Cooled Pebble Bed Breeding Blanket for the EU DEMO: Holistic Design Approach and Lessons Learned, Fusion Science and Technology, 75(5), pp. 352-364, 2019.

[16] E. Martelli et al., Advancements in DEMO WCLL breeding blanket design and integration, Int. J. Energy Res., 2018, 42; pp. 27-52.

[17] A. Tassone et al., Recent Progress in the WCLL Breeding Blanket Design for the DEMO Fusion Reactor, IEEE Trans. on Pl. Sc., 2018, 46, pp. 1446-1457.

[18] A. Del Nevo et al., Recent progress in developing a feasible and integrated conceptual design of the WCLL BB in EUROfusion project, Fus. Eng. Des. (2019), DOI: 10.1016/j.fusengdes.2019.03.040.

[19] J. Aubert et al., Status of the EU DEMO HCLL breeding blanket design development, Fus. Eng. Des., 2018, 136, Part B, 1428-1432.

[20] D. Rapisarda et al., Conceptual Design of the EU-DEMO Dual Coolant Lithium Lead Equatorial Module, IEEE Trans. on Pl. Sc., 2016, 44, pp. 1603-1612.

[21] G. Bongioví et al., Systems engineering activities supporting the heating & current drive and fuelling lines systems integration in the European DEMO breeding blanket, Fus. Eng. Des., 147, 111265, 2019.

[22] G. A. Spagnuolo et al., Systems Engineering approach in support to the breeding blanket design, Fus. Eng. Des., https://doi.org/10.1016/j.fusengdes.2018.11.016, 2018.

[23] G. Bongioví et al., Concept selection of the automated inspection and maintenance test unit for the EU DEMO using a novel fuzzy-based decision support tool, Fusion Engineering and Design, Volume 148, 2019, 111324.

[24] P. A. Di Maio et al., Structural analysis of the back supporting structure of the DEMO WCLL outboard blanket, Fus. Eng. Des. 124 (2017) 944-947.

[25] G. Zhou et al., Transient thermal analysis and structural

assessment of an ex-vessel LOCA event on the EU DEMO HCPB breeding blanket and the attachment system, Fus. Eng. Des., 136, 34-41, 2018.

[26] P. A. Di Maio et al., On the thermo-mechanical behavior of DEMO water-cooled lithium lead equatorial outboard blanket module, Fus. Eng. Des. 124 (2017) 725-729.

[27] G. Federici et al., European DEMO design strategy and consequences for materials, Nucl. Fusion 57 (2017), 092002.

[28] C. Bachmann, PDD-Plant Description Document v.1.3, https://idm.euro-fusion.org/?uid=2KVWQZ.

[29] C. Bachmann, PDD-Plant Description Document v.1.5, https://idm.euro-fusion.org/?uid=2KVWQZ.

[30] P. A. Di Maio et al., On the effect of stiffening plates configuration on the DEMO Water Cooled Lithium Lead Breeding Blanket module thermo-mechanical behavior, Fus. Eng. Des., https://doi.org/10.1016/j.fusengdes.2019.03.163, 2019.

[31] P. A. Di Maio et al., On the optimization of the first wall of the DEMO water-cooled lithium lead outboard breeding blanket equatorial module, Fus. Eng. Des., 109-111(PartA), pp. 335-341, 2016.

[32] R. Forte et al., Preliminary design of the top cap of DEMO Water-Cooled Lithium Lead breeding blanket segments, contribution at the 14th International Symposium on Nuclear Fusion Technology, Budapest, 22-27 September 2019.